

# Data-Driven Closed-Loop Reachability Analysis for Nonlinear Human-in-the-Loop Systems Using Gaussian Mixture Model

Joonwon Choi<sup>ID</sup>, *Graduate Student Member, IEEE*, Sooyung Byeon<sup>ID</sup>,  
and Inseok Hwang<sup>ID</sup>, *Member, IEEE*

**Abstract**—This article presents data-driven algorithms to perform the reachability analysis of nonlinear human-in-the-loop (HITL) systems. Such systems require consideration of the human control policy, otherwise might result in a conservative reachable set. However, formulating the human control policy in a mathematically tractable form is challenging, and thus, it is commonly ignored or simplified in many applications. To tackle this problem, we propose Gaussian mixture model (GMM)-based data-driven algorithms that can explicitly consider the human control policy during the reachability analysis of an HITL system. The proposed algorithms learn the human control policy as a GMM using the given trajectory. Then, the control input from the human operator is predicted based on the trained GMM by leveraging the Gaussian mixture regression (GMR), thereby facilitating the closed-loop forward stochastic reachability analysis. In this article, we examine two types of human control policies, state-independent and state-dependent, and propose the respective algorithms. We also tested our proposed algorithms using the human subject experimental data and demonstrated to generate more accurate results compared with other existing algorithms.

**Index Terms**—Data-driven modeling, human-in-the-loop (HITL), reachability analysis, vehicle safety.

## I. INTRODUCTION

THE human-in-the-loop (HITL) system is a system that includes one or more human operators within its control loop. Despite the recent advances in autonomous technology, some elements of human control are still desirable to correctly and safely operate a system [1], motivating active research on HITL systems such as the shared control [2], human–robot coexistence [3], and novice training [4]. The HITL system is especially safety-critical when a human operator physically interacts with the system. This brings the need for advanced safety analysis methods that can account for the human operator. To achieve this, various studies have been conducted to verify the safety of the HITL system [5].

Received 27 September 2023; revised 30 April 2024, 17 May 2024, and 18 October 2024; accepted 25 November 2024. Date of publication 24 December 2024; date of current version 25 February 2025. This work was supported by NSF under Grant CNS-1836952. Recommended by Associate Editor F. You. (*Corresponding author: Joonwon Choi*)

This work involved human subjects or animals in its research. Approval of all ethical and experimental procedures and protocols was granted by the Institutional Review Board (IRB) at Purdue University under Protocol No. IRB-2020-755.

The authors are with the School of Aeronautics and Astronautics, Purdue University, West Lafayette, IN 47907 USA (e-mail: choi774@purdue.edu; sbyeon@purdue.edu; ihwang@purdue.edu).

Digital Object Identifier 10.1109/TCST.2024.3518118

The reachability analysis is one of the widely used methods for the safety verification of HITL systems [6], [7], [8], [9], [10]. The reachability analysis can consider all the reachable states based on the system model, and thus, one can thoroughly examine the future operation of the target system. Nevertheless, the reachability analysis highly relies on the given system model. This might yield overly conservative results for HITL systems if the human operator’s behavior is not explicitly considered. For instance, a human driver is unlikely to get away from the road while driving, although it is included in the reachable set of a car. This can potentially lead to an overestimation of risk [11] which can be avoided by incorporating the human control policy into a reachable set computation. However, it is still a challenging task to formulate a complex human control policy in a mathematically tractable form.

The data-driven reachability analysis can be a proper solution for a system with black-box elements [11]. The data-driven reachability analysis uses trajectory data to compute the reachable set of a target system. Accordingly, a feasible result can be obtained without accurate knowledge of the target system. For instance, in [12], a data-driven approach was applied to estimate the reachable set of the system whose dynamics is learned as a neural network from a given set of trajectories. However, most of the existing data-driven reachability analysis methods aim to analyze the systems with uncertain parameters or unknown dynamics [13], [14], [15]. There have been relatively few works that consider the controller (human operator, for HITL systems) as a black-box element. Furthermore, if the dynamics of an HITL system is available, which is relatively easier to access than the human control policy, a pure data-driven algorithm without facilitating such side information might degrade its performance [16].

To address the previously mentioned limitations, we propose closed-loop data-driven forward stochastic reachability analysis algorithms for an HITL system. Unlike our previous works which deal with the linear dynamics [17], [18], we consider an HITL system with nonlinear dynamics. The HITL system is controlled by a human operator, and we model such a human operator’s control policy as a Gaussian mixture model (GMM) for the closed-loop reachability analysis of the HITL system. As a result, the proposed algorithms present a probability density function (pdf) of the future state of the HITL system,

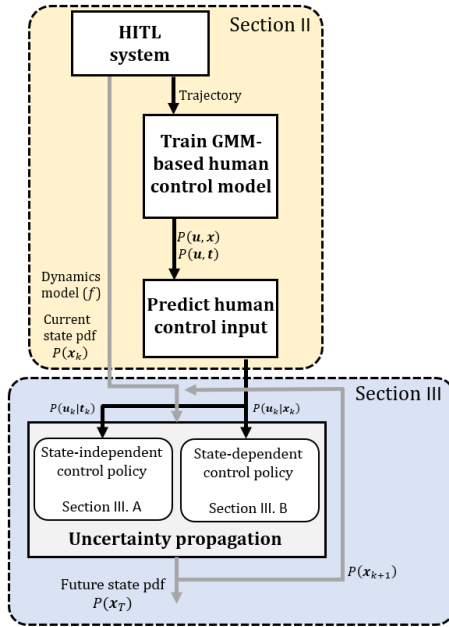


Fig. 1. Architecture of the proposed algorithm.

which provides more accurate and informative results compared with the existing methods by explicitly considering the human control policy. The architecture of the proposed algorithm is described in Fig. 1.

The GMM is a stochastic model that can represent human behavior more accurately compared with deterministic models by accounting for uncertainties inherent in human actions, such as the variability [19]. Thanks to this property, the GMM has been widely used to model the behavior of a driver [20], [21], [22], [23], [24], human limb motion [25], or to reproduce the most probable future state through imitation learning [26], [27], [28]. In our previous work [29], a bootstrapped GMM-based reachability analysis algorithm was proposed to account for the parameter estimation error when the dynamics of a target system is unavailable. In this study, we use the trained GMM to incorporate the human control policy for the reachability analysis by investigating potential human control actions and corresponding effects on the future operation of the HITL system.

The trained GMM represents the joint pdf between the system state (or time) and the control input from the human operator. Then, we use Gaussian mixture regression (GMR) to predict the control input from the human operator based on the trained GMM. The GMR is a computationally efficient algorithm that derives the conditional pdf on the control input, which is essential for predicting the evolution of the state over time. The state pdf at a specific future time instance can be computed by propagating the outcome of the GMR and the current state pdf according to the HITL system's dynamics. The predicted state pdf leverages the human control policy, thereby indicating *how likely the human operator drives the system to where* in the future, not simply representing which states are reachable.

We consider two types of human control policies: state-independent (open-loop) and state-dependent (closed-loop).

In modeling a driver's behavior in a near-accident situation, the control action of the driver (e.g., pedal or steering) can be modeled as a state-independent (open-loop) control [30], [31], [32]. On the other hand, the human control policy might be affected by the surrounding environment in routine or error adjustment operations, where the control policy is often expressed in a state-dependent (closed-loop) manner [30], [33]. Such modeling has been shown to be well-performed with the linear system in our previous works for both state-independent [17] and state-dependent [18] cases. Based on this, we propose data-driven algorithms for nonlinear HITL systems matched to these two cases and present human subject experiment results accordingly.

The main contribution of this article is twofolds: 1) we propose the data-driven algorithms to perform the closed-loop forward stochastic reachability analysis of a nonlinear HITL system. Extended from our previous works that leverage a GMM to analyze linear systems possibly with Gaussian noise [17], [18], the proposed algorithms can predict the future state pdf of a nonlinear HITL system with non-Gaussian noise, generalizing the application of the proposed framework to more broad types of problems. Leveraging the known dynamics of the target HITL system, as opposed to our previous work [29] where the dynamics information is unavailable, the proposed algorithms can explicitly account for a human control policy by learning it from data and 2) using data collected from human subject experiments, we demonstrate that the proposed algorithm can significantly reduce the conservativeness of existing methods, providing more accurate safety analysis results.

The remainder of this article is organized as follows. We present the GMM-based human control model in Section II. In Section III, the details of the proposed data-driven forward stochastic reachability analysis algorithms are provided. Finally, in Sections IV and V, the human subject experimental results and the conclusion are presented, respectively.

## II. GMM-BASED HUMAN CONTROL MODEL

We represent the human control policy as a GMM, a combination of multiple Gaussian elements, and use it to predict how the human operator controls the HITL system at a given state or time. Let a random variable  $\mathbf{r}$  be distributed by a GMM consisting of  $M$  Gaussian components, whose  $i$ th component is  $\pi_i N(\boldsymbol{\mu}_i, \Sigma_i)$  where  $N(\cdot, \cdot)$  is the Gaussian distribution,  $\pi_i$  is the weight of the  $i$ th Gaussian component satisfying  $\sum_{i=1}^M \pi_i = 1$ , and  $\boldsymbol{\mu}_i$  and  $\Sigma_i$  are the mean and covariance matrix, respectively. Then, the pdf of  $\mathbf{r}$  is represented as

$$P(\mathbf{r}) = \sum_{i=1}^M \pi_i N(\boldsymbol{\mu}_i, \Sigma_i). \quad (1)$$

We train the GMM to represent the joint pdf between  $\xi_{\text{out}} = [\xi_{\text{out},0}^T, \xi_{\text{out},1}^T, \dots, \xi_{\text{out},t_f}^T]^T$  and  $\xi_{\text{in}} = [\xi_{\text{in},0}^T, \xi_{\text{in},1}^T, \dots, \xi_{\text{in},t_f}^T]^T$ ,  $P(\xi_{\text{out}}, \xi_{\text{in}})$ , which we define as the *GMM-based human control model*  $\mathcal{H}$ . Here,  $t_f$  is the final time step of the trajectory and  $\xi_{\text{out},k} \in \mathbb{R}^l$  represents the data at time step  $k$  corresponding to the output that we want to predict for the

given input  $\xi_{\text{in},k} \in \mathbb{R}^g$ . More specifically, let  $\mathcal{H}$  be composed of  $M$  number of Gaussian components whose  $i$ th component's weight is  $\pi_{p,i}$  and mean ( $\mu_{p,i}$ ) and covariance ( $\Sigma_{p,i}$ ) are defined as

$$\mu_{p,i} = \begin{pmatrix} \mu_i^{\text{out}} \\ \mu_i^{\text{in}} \end{pmatrix}, \Sigma_{p,i} = \begin{pmatrix} \Sigma_i^{\text{out}} & \Sigma_i^{\text{out,in}} \\ \Sigma_i^{\text{in,out}} & \Sigma_i^{\text{in}} \end{pmatrix} \quad (2)$$

where  $\mu_i^{\text{out}} \in \mathbb{R}^l$  is the mean segment correlated with  $\xi_{\text{out}}$ ,  $\mu_i^{\text{in}} \in \mathbb{R}^g$  is that of  $\xi_{\text{in}}$ , and  $\Sigma_i^{\text{out}} \in \mathbb{R}^{l \times l}$ ,  $\Sigma_i^{\text{in}} \in \mathbb{R}^{g \times g}$ ,  $\Sigma_i^{\text{out,in}} \in \mathbb{R}^{l \times g}$ , and  $\Sigma_i^{\text{in,out}} \in \mathbb{R}^{g \times l}$  are the corresponding covariance segments, respectively. We define  $\mathcal{H}$  as follows.

*Definition 1:* The GMM-based human control model  $\mathcal{H}$  is a joint pdf between  $\xi_{\text{out}}$  and  $\xi_{\text{in}}$

$$\mathcal{H} := P(\xi_{\text{out}}, \xi_{\text{in}}) = \sum_i^M \pi_{p,i} N(\mu_{p,i}, \Sigma_{p,i}) \quad (3)$$

which has  $M$  number of Gaussian components.

The weight, mean, and covariance, i.e., parameters of  $\mathcal{H}$ , can be obtained by feeding  $\xi$  to a clustering algorithm (e.g., expectation–maximization (EM) algorithm) where  $\xi = [\xi_0^T, \xi_1^T, \dots, \xi_{I_f}^T]^T$  is the given trajectory of a target HITL system and  $\xi_k = [\xi_{\text{out},k}^T, \xi_{\text{in},k}^T]^T$  [26].

We use the trained  $\mathcal{H}$  to compute the conditional pdf  $P(\xi_{\text{out},k} | \xi_{\text{in},k})$  using the GMR. The computed  $P(\xi_{\text{out},k} | \xi_{\text{in},k})$  provides the prediction of the human operator's control input. For instance, let  $\xi_{\text{out},k} := \mathbf{u}_k$  and  $\xi_{\text{in},k} := t_k$ , where  $\mathbf{u}_k$  is the control input of an HITL system and  $t_k$  is the time at time step  $k$ . Then,  $P(\xi_{\text{out},k} | \xi_{\text{in},k}) = P(\mathbf{u}_k | t_k)$  can be considered as the predicted control input from the human operator at  $t_k$ , i.e., the state-independent human control policy. In the GMR, the conditional pdf  $P(\xi_{\text{out},k} | \xi_{\text{in},k})$  can be obtained as [26], [34]

$$P(\xi_{\text{out},k} | \xi_{\text{in},k}) = \sum_{i=1}^M \bar{\pi}_{p,i}(\xi_{\text{in},k}) N(\bar{\mu}_{p,i}(\xi_{\text{in},k}), \bar{\Sigma}_{p,i}) \quad (4)$$

where

$$\bar{\mu}_{p,i}(\xi_{\text{in},k}) = \mu_i^{\text{out}} + \Sigma_i^{\text{out,in}} \Sigma_i^{\text{in}^{-1}} (\xi_{\text{in},k} - \mu_i^{\text{in}}) \quad (5)$$

$$\bar{\Sigma}_{p,i} = \Sigma_i^{\text{out}} - \Sigma_i^{\text{out,in}} \Sigma_i^{\text{in}^{-1}} \Sigma_i^{\text{in,out}} \quad (6)$$

$$\bar{\pi}_{p,i}(\xi_{\text{in},k}) = \frac{\pi_i N(\xi_{\text{in},k} | \mu_i^{\text{in}}, \Sigma_i^{\text{in}})}{\sum_{j=1}^M \pi_j N(\xi_{\text{in},k} | \mu_j^{\text{in}}, \Sigma_j^{\text{in}})}. \quad (7)$$

Throughout this article, we assume  $\mathcal{H}$  is well-trained by the given trajectory of the HITL system so that it represents the true human control policy.

### III. DATA-DRIVEN CLOSED-LOOP REACHABILITY ANALYSIS OF NONLINEAR HITL SYSTEMS

In this section, we introduce the forward stochastic reachability analysis of an HITL system with a human operator considered as a state-independent and state-dependent controller, respectively.

#### A. Human as a State-Independent Controller

We consider the HITL system whose dynamics is given as a discrete-time nonlinear system

$$\mathbf{x}_{k+1} = f(\mathbf{x}_k, \mathbf{u}_k, \mathbf{v}_k) \quad (8)$$

where  $\mathbf{x}_k \in \mathbb{R}^n$  is the state vector at time step  $k$ ,  $\mathbf{u}_k \in \mathbb{R}^m$  is the input vector given by a human operator,  $\mathbf{v}_k \in \mathbb{R}^n$  is the (non-Gaussian) process noise, and  $f$  is the nonlinear system dynamics. Note that  $f$  is assumed to be known in this article. The proposed algorithms aim to predict the state pdf of an HITL system (8) at a desired future time step  $T > k$ ,  $P(\mathbf{x}_T)$ , while considering the human control policy by leveraging  $\mathcal{H}$ .

In this section, we assume the human control policy is state-independent.

*Assumption 1:* The human control policy is state-independent so that the human operator's control input ( $\mathbf{u}_k$ ) is independent of the state ( $\mathbf{x}_k$ ). In other words,  $\xi_{\text{in},k} = t_k$  and  $\xi_{\text{out},k} = \mathbf{u}_k$  where  $t_k = \Delta t \cdot k$  is the discrete-time instance and  $\Delta t$  is the discretization time interval.

If Assumption 1 holds, we can predict  $\mathbf{u}_k$  when  $t_k$  is given as

$$P(\mathbf{u}_k | t_k) = \sum_{i=1}^M \bar{\pi}_{p,i}(t_k) N(\bar{\mu}_{p,i}(t_k), \bar{\Sigma}_{p,i}) \quad (9)$$

where

$$\bar{\mu}_{p,i}(t_k) = \mu_i^{\text{out}} + \Sigma_i^{\text{out,in}} \Sigma_i^{\text{in}^{-1}} (\mathbf{u}_k - \mu_i^{\text{in}}) \quad (10)$$

$$\bar{\Sigma}_{p,i} = \Sigma_i^{\text{out}} - \Sigma_i^{\text{out,in}} \Sigma_i^{\text{in}^{-1}} \Sigma_i^{\text{in,out}} \quad (11)$$

$$\bar{\pi}_{p,i}(t_k) = \frac{\pi_i N(t_k | \mu_i^{\text{in}}, \Sigma_i^{\text{in}})}{\sum_{j=1}^M \pi_j N(t_k | \mu_j^{\text{in}}, \Sigma_j^{\text{in}})} \quad (12)$$

from (4)–(7) by setting  $\xi_{\text{in},k} = t_k$  and  $\xi_{\text{out},k} = \mathbf{u}_k$ .

Note that the future state of the HITL system becomes a random variable as  $\mathbf{u}_k$  is given as a random variable. One can compute the propagated state pdf  $P(\mathbf{x}_{k+1})$  of the HITL system (8) by solving the following equation [35]:

$$P(\mathbf{x}_{k+1}) = \int P(\mathbf{x}_{k+1} | \mathbf{x}_k) P(\mathbf{x}_k) d\mathbf{x}_k \quad (13)$$

where  $P(\mathbf{x}_{k+1} | \mathbf{x}_k)$  is called the transition kernel. Then,  $P(\mathbf{x}_T)$  can be obtained by iteratively solving (13).

$P(\mathbf{x}_{k+1})$  might not be distributed by a GMM even though  $P(\mathbf{x}_k)$  is distributed by a GMM due to the nonlinear dynamics and non-Gaussian process noise. Therefore, one needs to use a proper nonlinear uncertainty propagation algorithm to solve (13). For instance, the time update of the particle Gaussian mixture (PGM) filter [36] or modified ensemble Gaussian mixture filter (EnGMF) [37] can be suitable options. In this article, we use the modified EnGMF as an example [37]. The modified EnGMF algorithm is a hybrid algorithm of the particle filter and Gaussian sum filter. It is designed to track space objects with sparse observation data and thus suitable for propagating the state pdf for a long time without measurement [38]. The time update of the modified EnGMF starts by selecting  $N_E$  number of independent and identically distributed samples from the current state pdf  $P(\mathbf{x}_k)$ . The  $N_E$  samples approximate  $P(\mathbf{x}_k)$  as

$$P(\mathbf{x}_k) \approx \sum_{i=1}^{N_E} \frac{1}{N_E} \delta(\mathbf{x}_k - \mathbf{x}_k^{(i)}) \quad (14)$$

where  $\mathbf{x}_k^{(i)}$  is the  $i$ th sample and  $\delta$  is the Dirac delta function. As  $\delta(\cdot)$  can be considered as a Gaussian distribution with 0 covariance,  $N(\cdot, 0)$ , (14) can be regarded as the GMM with  $N_E$  number of Gaussian components with equal weights.

**Algorithm 1** Data-Driven Reachability Analysis of Nonlinear HITL System With Human as a State-Independent Controller

**Input:** initial state pdf  $P(\mathbf{x}_0)$ , dynamics (8),  $\mathcal{H}$ , arbitrary time step  $T > 0$ ,  $N_E$ , and  $\alpha_E$

**Output:**  $P(\mathbf{x}_T)$

```

while  $k < T$  do
     $i \leftarrow 1$ 
     $P(\mathbf{u}_k) \leftarrow$  prediction of human input from the GMR (9)
    while  $i < N_E + 1$  do
         $\mathbf{x}_k^{(i)} \leftarrow$  sample from the current state pdf,  $P(\mathbf{x}_k)$ 
         $\mathbf{x}_{k+1}^{(i)} \leftarrow$  sample from the transition kernel  $P(\cdot | \mathbf{x}_k^{(i)})$ 
         $i \leftarrow i + 1$ 
    end while
     $P(\mathbf{x}_{k+1}) \leftarrow$  approximated by  $N_E$  samples (15)-(16)
     $k \leftarrow k + 1$ 
end while

```

If Assumption 1 holds, the transition kernel  $P(\mathbf{x}_{k+1} | \mathbf{x}_k)$  can be rewritten as  $P(f(\mathbf{x}_k, \mathbf{u}_k, \mathbf{v}_k) | \mathbf{x}_k)$ . Then,  $P(\mathbf{x}_{k+1})$  can be approximated using the  $N_E$  samples as follows [37]:

$$P(\mathbf{x}_{k+1}) \approx \sum_{i=1}^{N_E} \frac{1}{N_E} N(\mathbf{x}_{k+1}^{(i)}, B_E) \quad (15)$$

where  $\mathbf{x}_{k+1}^{(i)}$  is computed by propagating  $\mathbf{x}_k^{(i)}$  according to the transition kernel  $P(f(\mathbf{x}_k, \mathbf{u}_k, \mathbf{v}_k) | \mathbf{x}_k)$ .  $B_E$  is the bandwidth matrix defined as

$$B_E = \alpha_E P_E \quad (16)$$

where  $0 \leq \alpha_E \leq 1$  is a design parameter and  $P_E$  is the sample covariance of the  $N_E$  samples [39]. One can propagate  $P(\mathbf{x}_k)$  to  $P(\mathbf{x}_T)$  by iteratively computing (15)–(16). The detailed algorithm of the proposed method is presented in Algorithm 1.

If the dynamics of the HITL system can be linearized as

$$\mathbf{x}_{k+1} = A\mathbf{x}_k + B\mathbf{u}_k + \mathbf{v}_k \quad (17)$$

where  $A \in \mathbb{R}^{n \times n}$  and  $B \in \mathbb{R}^{n \times m}$  are the system matrices, we can iteratively solve (13) by approximating  $\mathbf{v}_k$  as a GMM. It is widely known that any pdf can be approximated as closely as desired by a GMM through the Gaussian sum approximation [40], [41], [42]. In this article, we approximate  $\mathbf{v}_k$  by a GMM with  $L$  number of Gaussian components. The corresponding pdf of  $\mathbf{v}_k$  is given as

$$P(\mathbf{v}_k) \approx P(\hat{\mathbf{v}}_k) = \sum_{i=1}^L \pi_{v_k,i} N(\boldsymbol{\mu}_{v_k,i}, \Sigma_{v_k,i}) \quad (18)$$

where  $\pi_{v_k,i}$ ,  $\boldsymbol{\mu}_{v_k,i}$ , and  $\Sigma_{v_k,i}$  are the weight, mean, and covariance of the  $i$ th Gaussian component of  $\hat{\mathbf{v}}_k$ , respectively.

Let the state pdf be distributed by a GMM with  $G$  number of Gaussian components

$$P(\mathbf{x}_k) = \sum_{i=1}^G \pi_{x_k,i} N(\boldsymbol{\mu}_{x_k,i}, \Sigma_{x_k,i}). \quad (19)$$

Then, the linearized system (17) can be seen as a sum of three GMM random variables:  $A\mathbf{x}_k$ ,  $B\mathbf{u}_k$ , and  $\hat{\mathbf{v}}_k$ , and one can analytically compute the one-step propagation of its state pdf.

*Proposition 1:* If Assumption 1 holds and the dynamics of a target HITL system can be linearized as (17), the propagated

state pdf of the HITL system considering the state-independent human control policy,  $P(\mathbf{x}_{k+1})$ , is a GMM with MLG number of Gaussian components

$$P(\mathbf{x}_{k+1}) = \frac{1}{\eta} \sum_{i=1}^M \sum_{j=1}^L \pi_{t,i,j}(t_k) \sum_{l=1}^G \pi_{x_k,l} \\ \cdot N(A\boldsymbol{\mu}_{x_k,l} + \boldsymbol{\mu}_{t,i,j}(t_k), \Sigma_{t,i,j} + A\Sigma_{x_k,l}A^T). \quad (20)$$

*Proof:* The proof is provided in the Appendix. ■

The predicted  $P(\mathbf{x}_{k+1})$  from Proposition 1 indicates the probability distribution to which state the HITL system will be driven by the human operator represented as  $\mathcal{H}$ .

As shown in (48), the number of Gaussian components for the state pdf rapidly increases over time [43]. Such a growing number of Gaussian components needs to be alleviated to reduce the computation load [44]. In this article, we implement the method proposed in [45]. In [45], a reduced GMM  $P(\mathbf{x}_k^r)$  is computed by merging a pair of Gaussian components from  $P(\mathbf{x}_k)$ . Among all possible combinations, the pair that makes the minimum upper bound of the Kullback–Leibler (KL) divergence between the reduced GMM,  $P(\mathbf{x}_k^r)$ , and the current state GMM,  $P(\mathbf{x}_k)$ , is selected. Let  $(\pi_{x_k,i}, \pi_{x_k,j})$ ,  $(\boldsymbol{\mu}_{x_k,i}, \boldsymbol{\mu}_{x_k,j})$ , and  $(\Sigma_{x_k,i}, \Sigma_{x_k,j})$  be the pair of weights, means, and covariance matrices from the selected Gaussian components, respectively. The covariances are then merged as

$$\Sigma_{ij}^r = \frac{\pi_{x_k,i}}{\pi_{x_k,i} + \pi_{x_k,j}} \Sigma_{x_k,i} + \frac{\pi_{x_k,j}}{\pi_{x_k,i} + \pi_{x_k,j}} \Sigma_{x_k,j} \\ + \frac{\pi_{x_k,i}\pi_{x_k,j}}{(\pi_{x_k,i} + \pi_{x_k,j})^2} (\boldsymbol{\mu}_{x_k,i} - \boldsymbol{\mu}_{x_k,j})(\boldsymbol{\mu}_{x_k,i} - \boldsymbol{\mu}_{x_k,j})^T. \quad (21)$$

From (21), the upper bound of the KL divergence between  $P(\mathbf{x}_k^r)$  and  $P(\mathbf{x}_k)$ ,  $KL_{i,j}$ , is defined as follows:

$$KL_{i,j} = \frac{1}{2} \left[ (\pi_{x_k,i} + \pi_{x_k,j}) \ln(\det(\Sigma_{ij}^r)) \right. \\ \left. - \pi_{x_k,i} \ln(\det(\Sigma_{x_k,i})) - \pi_{x_k,j} \ln(\det(\Sigma_{x_k,j})) \right]. \quad (22)$$

The pair  $(i, j)$  that induces the minimum  $KL_{i,j}$  is selected among all the possible combinations and merged into a single Gaussian  $\pi_{ij}^r N(\boldsymbol{\mu}_{ij}^r, \Sigma_{ij}^r)$ , where  $\pi_{ij}^r = \pi_{x_k,i} + \pi_{x_k,j}$  and  $\boldsymbol{\mu}_{ij}^r = (\pi_{x_k,i}/\pi_{ij}^r)\boldsymbol{\mu}_{x_k,i} + (\pi_{x_k,j}/\pi_{ij}^r)\boldsymbol{\mu}_{x_k,j}$  [45]. The detailed algorithm for the linearized dynamics is shown in Algorithm 2.

### B. Human as a State-Dependent Controller

In this section, we consider the case where the human control policy is state-dependent.

*Assumption 2:* The human control policy is state-dependent so that the human operator's control input ( $\mathbf{u}_k$ ) is a function of the state ( $\mathbf{x}_k$ ),  $\mathbf{u}_k(\mathbf{x}_k)$ . In other words,  $\xi_{in,k} = \mathbf{x}_k$  and  $\xi_{out,k} = \mathbf{u}_k(\mathbf{x}_k)$ .

The dynamics of the HITL is given as

$$\mathbf{x}_{k+1} = f(\mathbf{x}_k, \mathbf{u}_k(\mathbf{x}_k), \mathbf{v}_k) \quad (23)$$

where  $\mathbf{u}_k(\mathbf{x}_k)$  is the state-dependent control input generated from the human operator. If Assumption 2 holds,

**Algorithm 2** Data-Driven Reachability Analysis of Linearized HITL System With Human as a State-Independent Controller  
**Input:** Initial state pdf  $P(\mathbf{x}_0)$ , linearized dynamics (17),  $\mathcal{H}$ , desired number of Gaussian components  $G_d$ , and arbitrary time step  $T > 0$   
**Output:**  $P(\mathbf{x}_T)$

```

while  $k < T$  do
     $P(\mathbf{u}_k) \leftarrow$  prediction of human input from the GMR (9)
     $P(\mathbf{x}_{k+1}) \leftarrow$  Propagated state pdf given in (48)
    while Number of Gaussian components of  $P(\mathbf{x}_{k+1}) > G_d$  do
        reduce the number of Gaussian components by using
        Gaussian reduction (21)-(22)
    end while
     $k \leftarrow k + 1$ 
end while

```

one can obtain the prediction of  $\mathbf{u}_k(\mathbf{x}_k)$  as a conditional pdf  $P(\xi_{\text{out},k}|\xi_{\text{in},k}) = P(\mathbf{u}_k|\mathbf{x}_k)$

$$P(\mathbf{u}_k|\mathbf{x}_k) = \sum_{i=1}^M \bar{\pi}'_{p,i}(\mathbf{x}_k) N(\bar{\mu}'_{p,i}(\mathbf{x}_k), \bar{\Sigma}'_{p,i}) \quad (24)$$

where

$$\bar{\mu}'_{p,i}(\mathbf{x}_k) = \boldsymbol{\mu}_i^{\text{out}} + \Sigma_i^{\text{out,in}} \Sigma_i^{\text{in}^{-1}} (\mathbf{x}_k - \boldsymbol{\mu}_i^{\text{in}}) \quad (25)$$

$$\bar{\Sigma}'_{p,i} = \Sigma_i^{\text{out}} - \Sigma_i^{\text{out,in}} \Sigma_i^{\text{in}^{-1}} \Sigma_i^{\text{in,out}} \quad (26)$$

$$\bar{\pi}'_{p,i}(\mathbf{x}_k) = \frac{\pi_i N(\mathbf{x}_k | \boldsymbol{\mu}_i^{\text{in}}, \Sigma_i^{\text{in}})}{\sum_{j=1}^M \pi_j N(\mathbf{x}_k | \boldsymbol{\mu}_j^{\text{in}}, \Sigma_j^{\text{in}})}. \quad (27)$$

Then,  $P(\mathbf{x}_{k+1})$  can be computed by solving (13) with the transition kernel

$$P(\mathbf{x}_{k+1}|\mathbf{x}_k) = P(f(\mathbf{x}_k, \mathbf{u}_k(\mathbf{x}_k), \mathbf{v}_k)|\mathbf{x}_k). \quad (28)$$

Analytically solving (13) with the transition kernel (28) is a challenging task. The nonlinear function (27) has  $\mathbf{x}_k$  as its variable, and thus, many existing nonlinear uncertainty propagation methods might not be directly applicable because of its state dependency. To address this, we adopt the PGM filter [36], [46]. The time update algorithm of the PGM filter can approximate the state pdf at a future time step using the samples propagated through the transition kernel. Assume  $N_P \in \mathbb{N}$  samples are used to propagate the state. The PGM filter algorithm takes  $N_P$  samples  $S_s^{(i)}, i = 1, 2, \dots, N_P$  from  $P(\mathbf{x}_k)$ . Then,  $S_s^{(i)}$  are propagated through the transition kernel (28) to compute  $S_s'^{(i)}$ . The propagated state pdf  $P(\mathbf{x}_{k+1})$  can be approximated as a GMM by clustering  $\{S_s'^{(i)} | i = 1, 2, \dots, N_P\}$ .

Note that  $P(\mathbf{x}_{k+1})$  can be approximated arbitrarily close as a GMM [40], [41], [42]. Let  $P(\hat{\mathbf{x}}_{k+1})$  be the Gaussian sum approximation of  $P(\mathbf{x}_{k+1})$  composed of  $G$  number of Gaussian components whose  $i$ th weight, mean, and covariance are  $\hat{\pi}_{x_{k+1},i}$ ,  $\hat{\mu}_{x_{k+1},i}$ , and  $\hat{\Sigma}_{x_{k+1},i}$ , respectively. Then, it was proved that there exists the number of samples that enables the PGM filter algorithm to approximate the parameters of  $P(\hat{\mathbf{x}}_{k+1})$  with desired accuracy and confidence.

*Lemma 1 (Time Update of PGM Filter [36]):* With the perfect clustering algorithm and given  $\epsilon' > 0$  and  $\delta' > 0$ ,

there exists the number of samples ( $N_P$ ) such that the time update of PGM filter can compute  $P(\hat{\mathbf{x}}_{k+1})$  which is the approximation of  $P(\hat{\mathbf{x}}_{k+1})$

$$P(\hat{\mathbf{x}}_{k+1}) = \sum_i^G \hat{\pi}_{x_{k+1},i} N(\hat{\mu}_{x_{k+1},i}, \hat{\Sigma}_{x_{k+1},i}) \quad (29)$$

that satisfies the following for all  $i = 1, 2, \dots, G$ :

$$\text{Prob}(|\hat{\pi}_{x_{k+1},i} - \hat{\pi}_{x_{k+1},i}| > \epsilon') < \delta' \quad (30)$$

$$\text{Prob}(\|\hat{\mu}_{x_{k+1},i} - \hat{\mu}_{x_{k+1},i}\|_2 > \epsilon') < \delta' \quad (31)$$

$$\text{Prob}(\|\hat{\Sigma}_{x_{k+1},i} - \hat{\Sigma}_{x_{k+1},i}\|_s > \epsilon') < \delta' \quad (32)$$

where  $\hat{\pi}_{x_{k+1},i}$ ,  $\hat{\mu}_{x_{k+1},i}$ , and  $\hat{\Sigma}_{x_{k+1},i}$  are the parameters, i.e., weight, mean, and covariance of the  $i$ th component of  $P(\hat{\mathbf{x}}_{k+1})$ ;  $\|\cdot\|_2$  is the 2-norm; and  $\|\cdot\|_s$  is the spectral norm.

One can refer [36] for the rigorous proof of Lemma 1.

*Proposition 2:* If Assumption 2 holds, with a perfect clustering algorithm and the number of samples ( $N_P$ ) corresponding to the desired accuracy and confidence, the approximation of state pdf of the HITL system at the desired future time step  $T$ ,  $P(\mathbf{x}_T)$ , can be computed with desired accuracy and confidence on its parameter while considering the state-dependent human control policy.

*Proof:* Lemma 1 automatically proves Proposition 2.

Without loss of generality, we consider the one-step propagation case. The propagated state pdf  $P(\mathbf{x}_{k+1})$  obtained using (28) considers the true state-dependent human control policy based on  $\mathcal{H}$ . Then,  $P(\hat{\mathbf{x}}_{k+1})$  can approximate  $P(\mathbf{x}_{k+1})$  arbitrarily close by the Gaussian sum approximation [40], [41], [42]. Furthermore, from Lemma 1, there exists the number of samples  $N_P$  such that the time update of the PGM filter can approximate the parameters of  $P(\hat{\mathbf{x}}_{k+1})$  with arbitrary accuracy and confidence. Thus, the true future state pdf of the HITL system  $P(\mathbf{x}_{k+1})$  can be approximated as  $P(\hat{\mathbf{x}}_{k+1})$  while considering the state-dependent human control policy. ■

Proposition 2 indicates that the proposed algorithm can achieve an accurate approximation of  $P(\mathbf{x}_T)$  while considering how the human operator drives the target HITL system. Algorithm 3 shows the detailed procedure of the proposed algorithm.

#### IV. HUMAN SUBJECT EXPERIMENTS

We conducted human subject experiments to test the performance of the proposed algorithms. We used three types of multirotor flight simulators set on the 2-D environment to collect the human data: two simulators for each dynamics (linearized, nonlinear) with a near-accident scenario to collect the state-independent flight data and one simulator with the nonlinear dynamics with a multiple routes scenario to collect the state-dependent flight data. The participants were asked to control a multirotor vehicle and complete given tasks in each simulation. Detailed information on each scenario and simulator is given later part of this section. A total of 16 participants were recruited for this study based on the following criteria: 1) 18 years of age or older; 2) have a normal or corrected-to-normal vision; and 3) have no known disorders or injuries

**Algorithm 3** Data-Driven Reachability Analysis of Nonlinear HITL System With Human as a State-Dependent Controller

**Input:** initial state pdf  $P(\mathbf{x}_0)$ , dynamics (23),  $\mathcal{H}$ , arbitrary time step  $T > 0$ , and  $N_P$

**Output:**  $P(\mathbf{x}_T)$

while  $k < T$  do

$i \leftarrow 1$

**for**  $i < N_P + 1$  **do**

$S_s^{(i)} \leftarrow$  sample from the current state pdf  $P(\mathbf{x}_k)$ , (19)

$P(\mathbf{u}_k(S_s^{(i)})) \leftarrow$  prediction of human input at given  $S_s^{(i)}$  from the GMR (24)

$S_s'^{(i)} \leftarrow$  samples from the transition kernel  $P(\cdot | S_s^{(i)})$  (28)

$i \leftarrow i + 1$

**end for**

$P(\hat{\mathbf{x}}_{k+1}) \leftarrow$  approximated from  $P(\hat{\mathbf{x}}_{k+1})$  clustered by the samples  $S_s'^{(i)}, \forall i = 1, 2, \dots, N_P$

$k \leftarrow k + 1$

**end while**

that may affect tactile sensitivity. A total of 811 trials of flight data were collected. We separated 15 trials for validation, five trials for each case, and the remaining data were used for training. As a result, three GMM-based human control models ( $\mathcal{H}$ ) were trained: the state-independent model for the linearized dynamics, the state-independent model for the nonlinear dynamics, and the state-dependent model for the nonlinear dynamics.

#### A. Experimental Scenarios

1) *Near-Accident Scenario*: In this scenario, the human operator acts as a state-independent controller of the multirotor, i.e., Assumption 1 holds. The simulation sets on a multirotor landing mission with a pop-up obstacle to collect the response of the participants in a near-accident situation. The concept of the scenario is illustrated in Fig. 2(a). The objective of this simulation is to safely land the multirotor on the touch pad located at the bottom. During the simulation, the participants were asked to follow the left lane and maintain a constant speed unless necessary to deviate to avoid a collision. The pop-up obstacle is spawned in a random location and the participants should avoid the obstacle otherwise the trial instantly ends. The GMM-based human control model  $\mathcal{H}$  is trained by the trajectories that are recorded during the participants' evasive maneuver to avoid the pop-up obstacle. The parameters used for the experiments are presented in Table I.

2) *Multiple Routes Scenario*: In this scenario, the human operator acts as a state-dependent controller of the multirotor, i.e., Assumption 2 holds. As shown in Fig. 2(b), the participants were asked to follow one of the two predefined routes and land the multirotor safely. The designated route was informed at the beginning of each simulation and the participants need to maintain a constant speed during the experiments.  $\mathcal{H}$  is trained using the trajectories recorded during the experiments. Accordingly, the trained  $\mathcal{H}$  includes the participants' state-dependent control policy that indicates

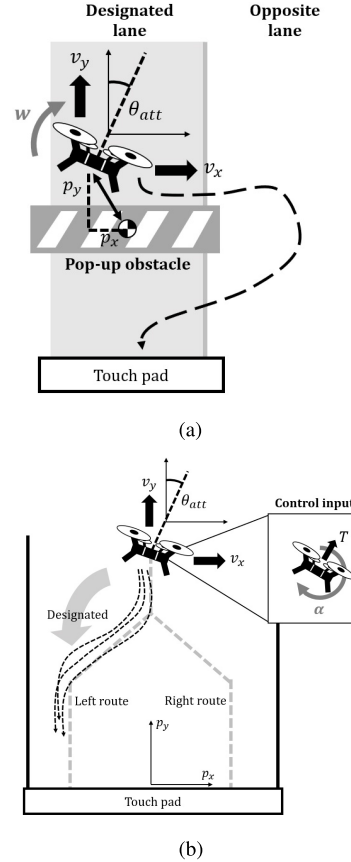


Fig. 2. Multirotor simulation scenarios for human subject experiments. (a) Multirotor landing mission in the near-accident scenario. (b) Multirotor landing mission in the multiple routes scenario.

TABLE I  
PARAMETERS FOR NEAR-ACCIDENT SCENARIO

Discretization time interval for linearized (nonlinear) dynamics ( $\Delta t$ )	0.04 (0.1) [s]
Gravitational acceleration ( $g$ )	9.8 [m/s <sup>2</sup> ]
Mass ( $m$ )	0.25 [kg]
Moment of inertia ( $I_x$ )	0.01 [kg · m <sup>2</sup> ]
Control parameter for linearized dynamics ( $c_{lin,1}, c_{lin,2}, c_{lin,3}$ )	-0.1, -1, -30
Control parameter for nonlinear dynamics ( $c_{non,1} - c_{non,7}$ )	60, -60, -0.5, 60, 60, 30, -0.2
Bound of thrust ( $T$ )	[-1.7, 1.7]
Bound of angular acceleration ( $\alpha$ )	[-0.5, 0.5]
Bound of X axis linear speed ( $v_x$ )	[-20, 20] [m/s]
Bound of Y axis linear speed ( $v_y$ )	[-15, 15] [m/s]
Number of Gaussian components of $\mathcal{H}$ ( $M$ )	6
Number of Gaussian components of state pdf ( $G$ )	6
Maximum number of Gaussian components ( $G_d$ )	6
Number of samples for comparative methods [47], [48]	2500
Number of samples for Monte Carlo simulation	20000
Parameter for modified EnGMMF ( $N_E, \alpha_E$ )	800, 0.0381

where the multirotor is headed. The parameters used for the experiments are presented in Table II.

#### B. Target System

We set the state vector at time step  $k$  as  $\mathbf{x}_k = [p_{x,k}, p_{y,k}, \theta_{att,k}, v_{x,k}, v_{y,k}, w_k]^T$ , where  $v_{x,k}$  and  $v_{y,k}$  are the X- and Y-axis linear velocity, respectively,  $\theta_{att,k}$  is the attitude,

TABLE II  
PARAMETERS FOR MULTIPLE ROUTES' SCENARIO

Discretization time interval ( $\Delta t$ )	0.1 [s]
Gravitational acceleration ( $g$ )	9.8 [m/s <sup>2</sup> ]
Mass ( $m$ )	0.25 [kg]
Moment of inertia ( $I_x$ )	0.01 [kg · m <sup>2</sup> ]
Control parameter for nonlinear dynamics ( $c_{non,1} - c_{non,7}$ )	60, -60, -0.5, 60, 60, 30, -0.2
Bound of thrust ( $T$ )	[-1.5, 1.5]
Bound of angular acceleration ( $\alpha$ )	[-0.6, 0.6]
Bound of X axis linear speed ( $v_x$ )	[-10, 10] [m/s]
Bound of Y axis linear speed ( $v_y$ )	[-15, 15] [m/s]
Number of Gaussian components of $\mathcal{H}$ ( $M$ )	6
Number of Gaussian components of state pdf ( $G$ )	6
Number of samples for comparative methods [47], [48]	2500
Number of samples for Monte Carlo simulation	20000
Number of samples for PGM filter ( $N_P$ )	500

and  $w_k$  is the angular velocity.  $p_{x,k}$  and  $p_{y,k}$  vary depending on the scenario. For the near-accident scenario, they are defined as the  $X$ - and  $Y$ -axes relative positions between the multirotor and the obstacle. For the multiple routes' scenario,  $p_{x,k}$  and  $p_{y,k}$  represent the  $X$ - and  $Y$ -axes positions of the multirotor, respectively. The control input is  $\mathbf{u}_k = [\alpha_k, T_k]^T$ , which consists of the angular acceleration ( $\alpha_k$ ) and the thrust ( $T_k$ ).

1) *Nonlinear Dynamics*: The nonlinear dynamics of the multirotor is defined as follows [4]:

$$\begin{aligned} T_{\text{total},k} &= c_{\text{non},1} T_k + c_{\text{non},2} + c_{\text{non},3} v_{y,k} \\ T_{\text{diff},k} &= c_{\text{non},4} \alpha_k + c_{\text{non},5} \theta_k + c_{\text{non},6} w_k + c_{\text{non},7} v_{x,k} \\ v_{x,k+1} &= v_{x,k} + \frac{T_{\text{total},k}}{m} \sin(\theta_k) \Delta t \\ v_{y,k+1} &= v_{y,k} + \left( \frac{T_{\text{total},k}}{m} \cos(\theta_k) - g \right) \Delta t \\ w_{k+1} &= w_k + \frac{T_{\text{diff},k}}{I_x} \Delta t \end{aligned} \quad (33)$$

where  $g$  is the gravitational acceleration,  $c_{\text{non},1} - c_{\text{non},7} \in \mathbb{R}$  are the controller parameters,  $m$  is the mass, and  $I_x$  and  $\Delta t$  are the moment of inertia of the multirotor and the discretization time interval, respectively.

2) *Linearized Dynamics*: The system matrices of the multirotor,  $A$  and  $B$ , are computed by linearizing the nonlinear dynamics of the multirotor at an equilibrium point [2], [49]

$$A = I_6 + \begin{pmatrix} 0 & 0 & 0 & 1 & 0 & 0 \\ 0 & 0 & 0 & 0 & 1 & 0 \\ 0 & 0 & 0 & 0 & 0 & 1 \\ 0 & 0 & g & 0 & 0 & 0 \\ 0 & 0 & 0 & 0 & c_{\text{lin},1} & 0 \\ 0 & 0 & c_{\text{lin},2} & 0 & 0 & c_{\text{lin},3} \end{pmatrix} \Delta t \quad (34)$$

$$B = \begin{pmatrix} 0 & 0 \\ 0 & 0 \\ 0 & 0 \\ 0 & 0 \\ 0 & 1/m \\ 1/I_x & 0 \end{pmatrix} \Delta t \quad (35)$$

where  $c_{\text{lin},1} - c_{\text{lin},3} \in \mathbb{R}$  are the controller parameters, and  $I_6$  is the  $6 \times 6$  identity matrix.

We present the human subject experiment results and compare the proposed algorithms with others. Two algorithms that can incorporate  $\mathcal{H}$  were selected for a fair comparison; the Monte Carlo sampling (MCS)-based method [47] and randUP [48]. The pdfs are properly truncated or marginalized according to the conditions. We also compare the results with the convex hull created from Monte Carlo samples without considering  $\mathcal{H}$ , i.e., assuming  $\mathbf{u}_k$  is uniformly distributed within the given bound.

### C. Experimental Results From Near-Accident Scenario

For both linearized and nonlinear dynamics cases, we assume there is initial state uncertainty distributed by a GMM  $\sum_{i=1}^3 \pi_{\text{noise},i} N(\boldsymbol{\mu}_{\text{noise},i}, \Sigma_{\text{noise},i})$  where

$$\pi_{\text{noise},i} = \frac{1}{3} \quad \forall i \quad (36)$$

$$\boldsymbol{\mu}_{\text{noise},1} = [0, 0, 0, 0, 0, 0]^T \quad (37)$$

$$\boldsymbol{\mu}_{\text{noise},2} = [1, 1, 0.1, 1, 1, 0.05]^T \quad (38)$$

$$\boldsymbol{\mu}_{\text{noise},3} = [-1, 1, -0.1, -1, -1, -0.05]^T \quad (39)$$

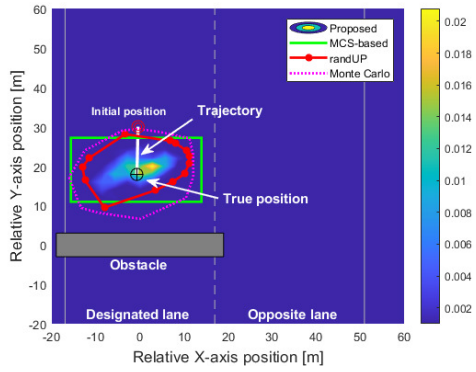
$$\Sigma_{\text{noise},i} = \text{diag}[1.5, 1.5, 0.05, 1, 2, 0.05] \quad \forall i. \quad (40)$$

Moreover, we define the collision probability,  $P_{\text{col}}$ , as the cumulative probability of the future state pdf over the pop-up obstacle.

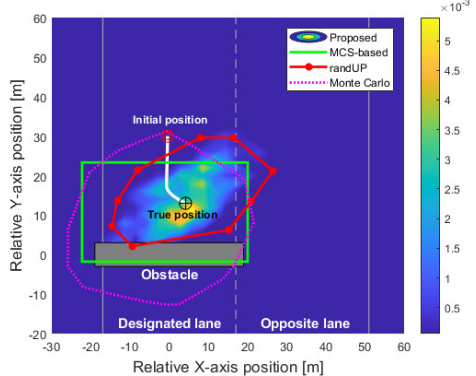
1) *Result From Nonlinear Dynamics Case*: The experimental results for the nonlinear dynamics are shown in Fig. 3, where the gray lines denote the lanes shown in Fig. 2(a), the box shows the pop-up obstacle, the red circle represents the position of the multirotor when the prediction starts, the black circle is the multirotor's true position at each specific future time, and the white line is the true trajectory. The contour describes the prediction result from the proposed algorithm (Algorithm 1). The convex hull drawn by the red line is the result of randUP [48], the green box is from the MCS-based method [47], and the purple convex hull is created by the Monte Carlo samples without considering  $\mathcal{H}$ .

One can observe from Fig. 3(a) to (e) that the predicted state pdf shows an irregular shape due to the nonlinear dynamics. Nevertheless, Algorithm 1 computes the accurate prediction result, successfully including the true position within its high probability region (bright area). Furthermore, it is clear that the proposed algorithm shows less conservative results. Especially, the proposed algorithm significantly alleviates the conservativeness compared with the convex hulls generated by the Monte Carlo samples. Furthermore, the proposed algorithm also shows benefits compared with the existing methods by providing additional probabilistic measures. In Fig. 3(c), the existing methods' reachable sets overlap with the pop-up obstacle indicating the multirotor could have a collision with the obstacle, whereas our proposed algorithm provides further probabilistic information showing that the collision probability is only 7.14%.

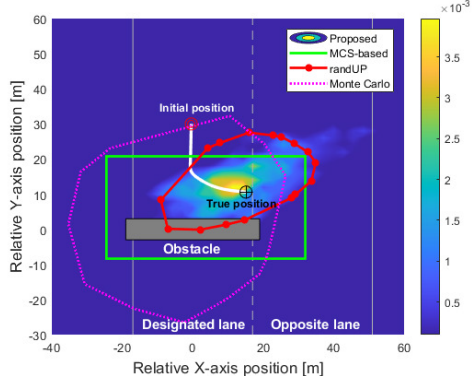
2) *Results From Linearized Dynamics Case*: The experimental results for the linearized dynamics (17) are shown in Fig. 4. We use Algorithm 2 to predict the state pdf at a desired future time instance. As observed in the case of nonlinear dynamics, the proposed algorithm computes significantly



(a)



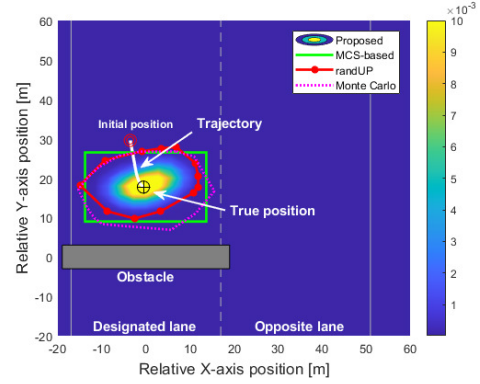
(b)



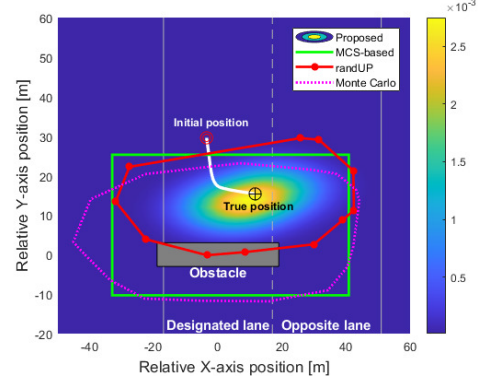
(c)

Fig. 3. Experimental results for the near-accident scenario with the nonlinear dynamics. The contour is the result of the proposed method and the colored lines represent those of the comparative methods. While the comparative methods generate overly conservative prediction results that include the obstacle inside, the proposed algorithm generates more accurate and thus practical results through the closed-loop analysis, indicating low collision probability. (a)  $t = 1.5$  s,  $P_{\text{col}} = 8.27e^{-91}$ . (b)  $t = 3$  s,  $P_{\text{col}} = 0.0538$ . (c)  $t = 4$  s,  $P_{\text{col}} = 0.0714$ .

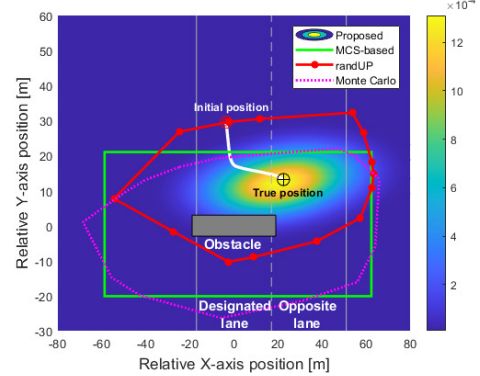
less conservative results in comparison to other methods. Particularly, in Fig. 4(b) and (c), the proposed algorithm indicates that the multirotor has only 2.27% and 6.89% of  $P_{\text{col}}$ , respectively, whereas the other comparative methods overlap with or even entirely include the obstacle. Such probabilistic information can provide benefits in analyzing the imminent danger of an HITL system. For instance, the less conservative result from the proposed algorithm can reduce false alarms by distinguishing risky, yet barely chosen control choices from the



(a)



(b)



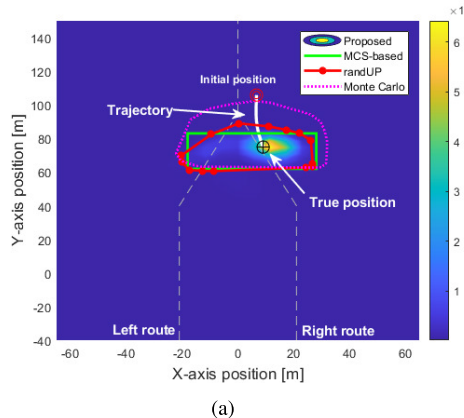
(c)

Fig. 4. Experimental results for the near-accident scenario with the linearized dynamics. A similar trend to the previous simulation can be observed. The proposed algorithm still predicts low collision probability, showing less conservative results compared with other comparative methods. (a)  $t = 1.5$  s,  $P_{\text{col}} = 4.07e^{-8}$ . (b)  $t = 3$  s,  $P_{\text{col}} = 0.0227$ . (c)  $t = 4$  s,  $P_{\text{col}} = 0.0689$ .

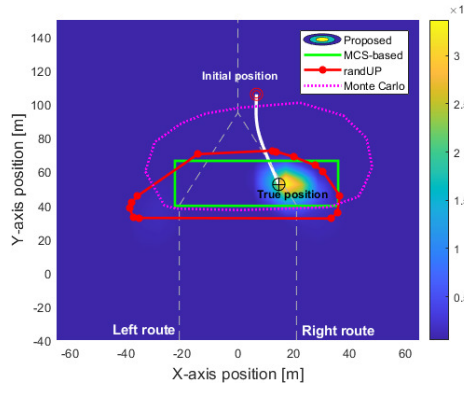
human operator. The proposed algorithm might also preserve trust in an assisting autonomy by realizing the minimum intervention, i.e., allowing its engagement only in a truly dangerous situation as opposed to frequently interrupting the human operator by the existing methods.

#### D. Experimental Results From Multiple Routes' Scenario

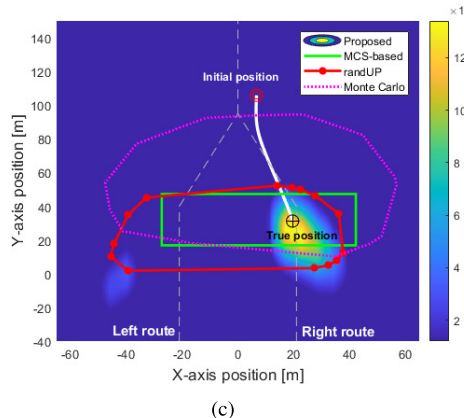
Figs. 5 and 6 show the experiment results for the multirotor with the nonlinear dynamics. Fig. 5 is the result when the human operator is designated to follow the right route, whereas Fig. 6 is that of the left route. Same as in Section IV-C, we assume there is initial uncertainty



(a)



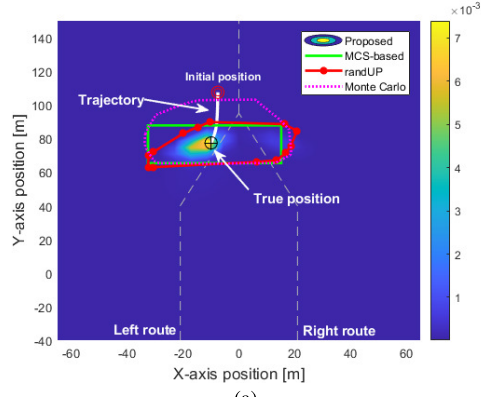
(b)



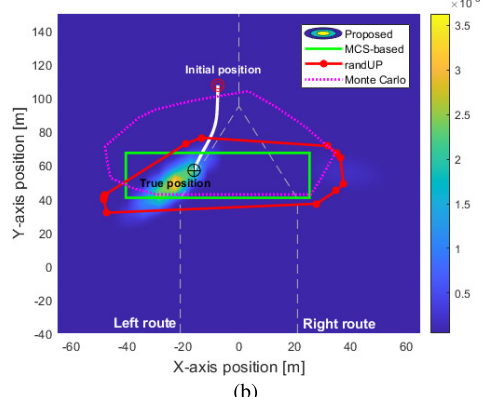
(c)

Fig. 5. Experimental results for the multiple routes' scenario with the nonlinear dynamics (right route). The contour is the result of the proposed method and the colored lines represent those of the comparative methods. The comparative methods produce overly conservative results that include both the lanes, whereas the proposed algorithm can distinguish the direction of the vehicle by explicitly considering human control policy. (a)  $t = 3$  s. (b)  $t = 5$  s. (c)  $t = 7$  s.

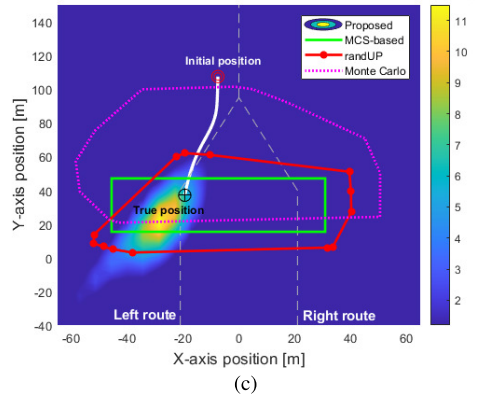
distributed by a GMM (36)–(40). In the figure, the red convex hull and green box are the results of randUP [48] and the MCS-based method [47], respectively, and the purple convex hull is constructed with the Monte Carlo simulation's samples. The red circle represents the initial position where the prediction begins, the black circle indicates the true multirotor location at each future time, and the white line is the multirotor's true trajectory. The gray dashed line represents the predefined route shown in Fig. 2(b). The colored contour is the result of the proposed algorithm which is computed with Algorithm 3.



(a)



(b)



(c)

Fig. 6. Experimental results for the multiple routes' scenario with the non-linear dynamics (left route). Similar to the previous simulation, the proposed algorithm can successfully capture that the vehicle headed in the opposite direction. This shows the proposed algorithm's capability of closed-loop analysis, i.e., leveraging the control strategy of the human operator. (a)  $t = 3$  s. (b)  $t = 5$  s. (c)  $t = 7$  s.

In the figure, one can find that the other comparative methods create large redundant areas that include both the routes. On the contrary, the proposed algorithm distinguishes the appropriate route where the multirotor is headed based on  $\mathcal{H}$ . In Fig. 5, it is obvious that the computed state pdf is concentrated on the right route while it is on the left route in Fig. 6, thereby significantly alleviating the conservativeness compared with other existing methods. Furthermore, the proposed algorithm provides probabilistic information concerning the future state of the multirotor and successfully predicts its position by assigning higher weights near the true location

of the multirotor. Such characteristics can provide significant benefits for analyzing the safety of an HITL system in real-world applications, especially when a human operator has multiple control choices. For instance, the conventional reachability analysis method might generate an overly conservative result for a car driving on a highway by including other lanes, although the driver does not have the intention to change lanes. Meanwhile, our proposed algorithm can infer the driver's behavior by incorporating the human control policy from  $\mathcal{H}$ . Consequently, the proposed algorithm can alleviate the false alarms that originated from the conservative reachable set, enhancing trust in the safety analysis result.

## V. CONCLUSION

In this article, we proposed data-driven algorithms to perform the forward stochastic reachability analysis of nonlinear HITL systems while explicitly considering a human control policy. Based on the fact that the human control policy can be represented in a state-independent or state-dependent manner, the proposed algorithms learn the human control policy as a GMM using the trajectory data generated from a target HITL system. The future state pdf is then computed based on the predicted control input pdf computed by the GMR. Through human subject experiments, the proposed algorithms were shown to generate more accurate and less conservative results in comparison to other existing methods.

In future work, we will investigate the online adaptation of the human control model. In many real-world applications, the human control policy may vary over time or be forced to change due to external environment. To address such a dynamic transition of the human control policy, we will leverage the online adaptation of the trained GMM using newly added measurement.

## APPENDIX PROOF OF PROPOSITION 1

From the linearized dynamics (17) and the Gaussian sum approximation, the transition kernel  $P(\mathbf{x}_{k+1}|\mathbf{x}_k)$  can be rewritten as

$$P(\mathbf{x}_{k+1}|\mathbf{x}_k) \approx P(A\mathbf{x}_k + B\mathbf{u}_k + \hat{\mathbf{v}}_k|\mathbf{x}_k). \quad (41)$$

Then, by incorporating the predicted control input pdf from the GMR (9), the transition kernel becomes

$$\begin{aligned} & P(A\mathbf{x}_k + B\mathbf{u}_k + \hat{\mathbf{v}}_k|\mathbf{x}_k) \\ &= \sum_{i=1}^M \sum_{j=1}^L \pi_{t,i,j}(t_k) N(A\mathbf{x}_k + \mu_{t,i,j}(t_k), \Sigma_{t,i,j}) \end{aligned} \quad (42)$$

where

$$\pi_{t,i,j}(t_k) = \bar{\pi}_{p,i}(t_k) \pi_{v_k,j} \quad (43)$$

$$\mu_{t,i,j}(t_k) = B\bar{\mu}_{p,i}(t_k) + \mu_{v_k,j} \quad (44)$$

$$\Sigma_{t,i,j} = B\bar{\Sigma}_{p,i}B^T + \Sigma_{v_k,j}. \quad (45)$$

By substituting (42) for  $P(\mathbf{x}_{k+1}|\mathbf{x}_k)$  in (13), one can obtain  $P(\mathbf{x}_{k+1})$

$$= \int \sum_{i=1}^M \sum_{j=1}^L \pi_{t,i,j}(t_k) N(A\mathbf{x}_k + \mu_{t,i,j}(t_k), \Sigma_{t,i,j}) P(\mathbf{x}_k) d\mathbf{x}_k \quad (46)$$

and from (19)

$$\begin{aligned} P(\mathbf{x}_{k+1}) &= \int \sum_{i=1}^M \sum_{j=1}^L \pi_{t,i,j}(t_k) N(A\mathbf{x}_k + \mu_{t,i,j}(t_k), \Sigma_{t,i,j}) \\ &\quad \cdot \sum_{l=1}^G \pi_{x_k,l} N(\mu_{x_k,l}, \Sigma_{x_k,l}) d\mathbf{x}_k. \end{aligned} \quad (47)$$

From [43], (47) can be rewritten as a GMM with MLG number of Gaussian components

$$\begin{aligned} P(\mathbf{x}_{k+1}) &= \frac{1}{\eta} \sum_{i=1}^M \sum_{j=1}^L \pi_{t,i,j}(t_k) \sum_{l=1}^G \pi_{x_k,l} \\ &\quad \cdot N(A\mu_{x_k,l} + \mu_{t,i,j}(t_k), \Sigma_{t,i,j} + A\Sigma_{x_k,l}A^T) \end{aligned} \quad (48)$$

where  $\eta$  is a constant that makes integral of (48) as 1 [43]. One can iteratively compute  $P(\mathbf{x}_T)$  using (48). ■

## REFERENCES

- [1] W. Li, D. Sadigh, S. S. Sastry, and S. A. Seshia, "Synthesis for human-in-the-loop control systems," in *Proc. Tools Algorithms Construction Anal. Syst. (TACAS)*, Jan. 2014, pp. 470–484.
- [2] S. Byeon, D. Sun, and I. Hwang, "Skill-level-based hybrid shared control for human-automation systems," in *Proc. IEEE Int. Conf. Syst., Man, Cybern. (SMC)*, Oct. 2021, pp. 1507–1512.
- [3] M. Ragaglia, A. M. Zanchettin, and P. Rocco, "Safety-aware trajectory scaling for human–robot collaboration with prediction of human occupancy," in *Proc. Int. Conf. Adv. Robot. (ICAR)*, Jul. 2015, pp. 85–90.
- [4] S. Byeon, W. Jin, D. Sun, and I. Hwang, "Human-automation interaction for assisting novices to emulate experts by inferring task objective functions," in *Proc. IEEE/AIAA Digital Avionics Syst. Conf. (DASC)*, Oct. 2021, pp. 1–6.
- [5] A. Pereira and M. Althoff, "Overapproximative human arm occupancy prediction for collision avoidance," *IEEE Trans. Autom. Sci. Eng.*, vol. 15, no. 2, pp. 818–831, Apr. 2018.
- [6] Y. Gao, F. J. Jiang, L. Xie, and K. H. Johansson, "Risk-aware optimal control for automated overtaking with safety guarantees," *IEEE Trans. Control Syst. Technol.*, vol. 30, no. 4, pp. 1460–1472, Jul. 2022.
- [7] A. Bajcsy, S. Bansal, E. Ratner, C. J. Tomlin, and A. D. Dragan, "A robust control framework for human motion prediction," *IEEE Robot. Autom. Lett.*, vol. 6, no. 1, pp. 24–31, Jan. 2021.
- [8] J. F. Fisac et al., "Probabilistically safe robot planning with confidence-based human predictions," 2018, *arXiv:1806.00109*.
- [9] S. R. Schepp, J. Thumm, S. B. Liu, and M. Althoff, "SaRA: A tool for safe human–robot coexistence and collaboration through reachability analysis," in *Proc. Int. Conf. Robot. Autom. (ICRA)*, May 2022, pp. 4312–4317.
- [10] K. Leung et al., "On infusing reachability-based safety assurance within planning frameworks for human–robot vehicle interactions," *Int. J. Robot. Res.*, vol. 39, nos. 10–11, pp. 1326–1345, Aug. 2020.
- [11] A. J. Thorpe and M. M. K. Oishi, "Model-free stochastic reachability using kernel distribution embeddings," *IEEE Control Syst. Lett.*, vol. 4, no. 2, pp. 512–517, Apr. 2020.
- [12] O. Thapliyal and I. Hwang, "Approximating reachable sets for neural network-based models in real time via optimal control," *IEEE Trans. Control Syst. Technol.*, vol. 31, no. 4, pp. 1901–1908, Jul. 2023.
- [13] A. Alanwar, A. Koch, F. Allgöwer, and K. H. Johansson, "Data-driven reachability analysis using matrix zonotopes," in *Proc. 3rd Conf. Learn. Dyn. Control*, 2021, pp. 163–175.
- [14] O. Thapliyal and I. Hwang, "Approximate reachability for Koopman systems using mixed monotonicity," *IEEE Access*, vol. 10, pp. 84754–84760, 2022.
- [15] A. Alanwar, A. Koch, F. Allgöwer, and K. H. Johansson, "Data-driven reachability analysis from noisy data," 2021, *arXiv:2105.07229*.
- [16] A. J. Thorpe, C. Neary, F. Djemou, M. M. K. Oishi, and U. Topcu, "Physics-informed kernel embeddings: Integrating prior system knowledge with data-driven control," 2023, *arXiv:2301.03565*.
- [17] J. Choi, S. Byeon, and I. Hwang, "State prediction of human-in-the-loop multi-rotor system with stochastic human behavior model," *IFAC-PapersOnLine*, vol. 55, no. 41, pp. 119–124, 2022.

- [18] J. Choi, S. Byeon, and I. Hwang, "Data-driven forward stochastic reachability analysis for human-in-the-loop systems," in *Proc. 62nd IEEE Conf. Decis. Control (CDC)*, Dec. 2023, pp. 1730–1735.
- [19] D. Koert, J. Pajarinen, A. Schotschneider, S. Trick, C. Rothkopf, and J. Peters, "Learning intention aware online adaptation of movement primitives," *IEEE Robot. Autom. Lett.*, vol. 4, no. 4, pp. 3719–3726, Oct. 2019.
- [20] P. Angkititrakul, R. Terashima, and T. Wakita, "On the use of stochastic driver behavior model in lane departure warning," *IEEE Trans. Intell. Transp. Syst.*, vol. 12, no. 1, pp. 174–183, Mar. 2011.
- [21] P. Angkititrakul, C. Miyajima, and K. Takeda, "Modeling and adaptation of stochastic driver-behavior model with application to car following," in *Proc. IEEE Intell. Vehicles Symp. (IV)*, Jun. 2011, pp. 814–819.
- [22] C.-H. Yang, C.-C. Chang, and D. Liang, "A novel GMM-based behavioral modeling approach for smartwatch-based driver authentication," *Sensors*, vol. 18, no. 4, p. 1007, Mar. 2018.
- [23] C. Miyajima et al., "Driver modeling based on driving behavior and its evaluation in driver identification," *Proc. IEEE*, vol. 95, no. 2, pp. 427–437, Feb. 2007.
- [24] R. Huang, H. Liang, P. Zhao, B. Yu, and X. Geng, "Intent-estimation- and motion-model-based collision avoidance method for autonomous vehicles in urban environments," *Appl. Sci.*, vol. 7, no. 5, p. 457, Apr. 2017.
- [25] Y. Huo, X. Li, X. Zhang, X. Li, and D. Sun, "Adaptive intention-driven variable impedance control for wearable robots with compliant actuators," *IEEE Trans. Control Syst. Technol.*, vol. 31, no. 3, pp. 1308–1323, May 2023.
- [26] S. Calinon, "A tutorial on task-parameterized movement learning and retrieval," *Intell. Service Robot.*, vol. 9, no. 1, pp. 1–29, 2016.
- [27] T. Osa, J. Pajarinen, G. Neumann, J. A. Bagnell, P. Abbeel, and J. Peters, "An algorithmic perspective on imitation learning," *Found. Trends Robot.*, vol. 7, nos. 1–2, pp. 1–179, 2018.
- [28] S. El Zaatar, W. Li, and Z. Usman, "Ring Gaussian mixture modelling and regression for collaborative robots," *Robot. Auto. Syst.*, vol. 145, Nov. 2021, Art. no. 103864.
- [29] J. Choi, H. Park, and I. Hwang, "Bootstrapped Gaussian mixture model-based data-driven forward stochastic reachability analysis," *IEEE Control Syst. Lett.*, vol. 8, pp. 1–6, 2024.
- [30] G. Markkula, "Modeling driver control behavior in both routine and near-accident driving," in *Proc. Human Factors Ergonom. Soc. Annu. Meeting*, Sep. 2014, vol. 58, no. 1, pp. 879–883.
- [31] G. Markkula, O. Benderius, and M. Wahde, "Comparing and validating models of driver steering behaviour in collision avoidance and vehicle stabilisation," *Vehicle Syst. Dyn.*, vol. 52, no. 12, pp. 1658–1680, Dec. 2014.
- [32] K. D. Kusano and H. C. Gabler, "Safety benefits of forward collision warning, brake assist, and autonomous braking systems in rear-end collisions," *IEEE Trans. Intell. Transp. Syst.*, vol. 13, no. 4, pp. 1546–1555, Dec. 2012.
- [33] M. Martínez-García, Y. Zhang, and T. Gordon, "Modeling lane keeping by a hybrid open-closed-loop pulse control scheme," *IEEE Trans. Ind. Informat.*, vol. 12, no. 6, pp. 2256–2265, Dec. 2016.
- [34] F. Stulp and O. Sigaud, "Many regression algorithms, one unified model: A review," *Neural Netw.*, vol. 69, pp. 60–79, Sep. 2015.
- [35] G. Terejanu, P. Singla, T. Singh, and P. D. Scott, "Uncertainty propagation for nonlinear dynamic systems using Gaussian mixture models," *J. Guid., Control, Dyn.*, vol. 31, no. 6, pp. 1623–1633, Nov. 2008.
- [36] D. Raihan and S. Chakravorty, "Particle Gaussian mixture filters-I" *Automatica*, vol. 98, pp. 331–340, Dec. 2018.
- [37] S. Yun, "Sequential Monte Carlo filtering with Gaussian mixture models for highly nonlinear systems," Ph.D. dissertation, Dept. Aerosp. Eng. Mech., Univ. Texas Austin, Austin, TX, USA, 2021.
- [38] S. Yun, R. Zanetti, and B. A. Jones, "Kernel-based ensemble Gaussian mixture filtering for orbit determination with sparse data," *Adv. Space Res.*, vol. 69, no. 12, pp. 4179–4197, Jun. 2022.
- [39] B. Liu, B. Ait-El-Equih, and I. Hoteit, "Efficient kernel-based ensemble Gaussian mixture filtering," *Monthly Weather Rev.*, vol. 144, no. 2, pp. 781–800, Feb. 2016.
- [40] J. T. Horwood, N. D. Aragon, and A. B. Poore, "A Gaussian sum filter framework for space surveillance," *Proc. SPIE*, vol. 8137, pp. 186–197, Sep. 2011.
- [41] H. Sorenson and D. Alspach, "Recursive Bayesian estimation using Gaussian sums," *Automatica*, vol. 7, no. 4, pp. 465–479, 1971.
- [42] K. Ito and K. Xiong, "Gaussian filters for nonlinear filtering problems," *IEEE Trans. Autom. Control*, vol. 45, no. 5, pp. 910–927, May 2000.
- [43] A. Karumanchi and P. Tulpule, "Comparing linear systems with Gaussian mixture model additive uncertainties using Kullback–Leibler rate," *IFAC-PapersOnLine*, vol. 54, no. 20, pp. 566–572, 2021.
- [44] Q. Zhang, A. Gong Zhang, and J. Chen, "Gaussian mixture reduction with composite transportation divergence," 2020, *arXiv:2002.08410*.
- [45] A. R. Runnalls, "Kullback–Leibler approach to Gaussian mixture reduction," *IEEE Trans. Aerosp. Electron. Syst.*, vol. 43, no. 3, pp. 989–999, Jul. 2007.
- [46] D. Raihan and S. Chakravorty, "Particle Gaussian mixture filters-II," *Automatica*, vol. 98, pp. 341–349, Dec. 2018.
- [47] A. Devonport and M. Arcak, "Data-driven reachable set computation using adaptive Gaussian process classification and Monte Carlo methods," in *Proc. IEEE Amer. Control Conf.*, Jul. 2020, pp. 2629–2634.
- [48] T. Lew and M. Pavone, "Sampling-based reachability analysis: A random set theory approach with adversarial sampling," in *Proc. Conf. Robot Learn.*, 2021, pp. 2055–2070.
- [49] F. Sabatino, "Quadrotor control: Modeling, nonlinear control design, and simulation," M.S. thesis, KTH Royal Inst. Technol., Stockholm, Sweden, 2015.



**Joonwon Choi** (Graduate Student Member, IEEE) received the bachelor's degree in mechanical and aerospace engineering and the master's degree in mechanical engineering from Ulsan National Institute of Science and Technology (UNIST), Ulsan, South Korea, in 2019 and 2021, respectively.

He was a Researcher with the Autonomous Systems Laboratory, UNIST, from 2019 to 2020. He is currently a Research Assistant with the School of Aeronautics and Astronautics, Purdue University, West Lafayette, IN, USA. His research interests include human–automation interaction, data-driven reachability analysis, and applied experiments.



**Sooyoung Byeon** received the bachelor's and master's degrees in aerospace engineering from Korea Advanced Institute of Science and Technology (KAIST), Daejeon, Republic of Korea, in 2012 and 2014, respectively.

He was a Senior Research Engineer at Satrec Initiative Company Ltd., Daejeon, from 2014 to 2019. He is currently a Research Assistant with the School of Aeronautics and Astronautics, Purdue University, West Lafayette, IN, USA. His research interests include human–automation interaction, human behavior modeling, imitation learning, and applied experiments.



**Inseok Hwang** (Member, IEEE) received the Ph.D. degree in aeronautics and astronautics from Stanford University, Stanford, CA, USA, in 2004.

He is a Professor with the School of Aeronautics and Astronautics, Purdue University, West Lafayette, IN, USA. His research interests include modeling, estimation, and control of cyber-physical systems and their applications to safety critical systems such as aircraft/spaceship/unmanned aerial systems, air traffic management, and multiagent systems. For his research, he leads the Flight Dynamics and Control/Hybrid Systems Laboratory, Purdue University.